ADVANCED MATERIALS INTERFACES
Open Access
www.advmatinterfaces.de

Check for updates

Revitalizing Inert Materials: Grafting Self-Oscillating, Stimuli-Responsive Organometallic Polymers for Pulsating Systems

*Johanne Pirkin-Benameur, Vincent Bouad, Flora Lefèbvre, Denis Bouyer, Katell Sénéchal-David, Jean-Noël Rebilly, Frédéric Banse, David Fournier, Patrice Woisel, Joël Lyskawa, and Damien Quemener**

A major challenge in materials science is dynamically adjusting material properties using sensors and control systems. This contribution develops a new approach using a self-oscillating copolymer to autonomously change material surface properties in response to environmental changes. A redox-sensitive terpolymer of *N*-isopropylacrylamide (NIPAM), dimethylacrylamide (DMAc), and an iron-based comonomer ([(phen)$_2$(phen-5-yl-acrylamide)Fe^{II}](PF$_6$)$_2$) is synthesized via Reversible Addition-Fragmentation Chain Transfer (RAFT) polymerization, catalyzing an oscillating redox reaction (Belousov-Zhabotinsky, BZ). The terpolymer oscillates from soluble to insoluble around 35 °C based on the iron's oxidation state. A catechol unit is incorporated to enhance versatility, enabling grafting onto different surfaces. Optimal BZ reagent concentrations are explored for maximum oscillation amplitude and frequency. By selecting a working temperature between redox transition points, the copolymer's oscillation from coil to globular conformation is observed due to redox oscillations. The self-oscillating copolymer is grafted onto an ultrafiltration membrane, where conformational changes cause variations in pore size, leading to rapid negative flux peaks that disrupt the flux and reduce membrane fouling during protein filtration. This study highlights self-oscillating polymers' ability to impart dynamic properties to inert materials, paving the way for smart materials with self-regulating properties to adapt to changing conditions.

1. Introduction

Polymeric materials, initially derived from natural sources, have progressed significantly through chemical modifications, resulting in improved functional properties and new applications in everyday life. A new generation of stimuli-responsive polymers has emerged to address current challenges.[1] These materials can undergo predictable changes at the molecular level, achieving a degree of autonomy. Applications of stimuli-responsive polymers include drug delivery systems,[2,3] hydrogels,[4,5] sensors,[6,7] and artificial muscles.[8] Stimuli such as pH,[9–10] temperature,[11] magnetic,[12] or electric fields,[13] light,[14] or the presence of certain molecules have been studied.[15]

One of the most studied thermosensitive polymers is poly(*N*-isopropylacrylamide) (PNIPAM), which transitions from a water-soluble coil to a water-insoluble globular conformation above a threshold temperature (Low Critical Solution Temperature, LCST) of about

J. Pirkin-Benameur, D. Bouyer, D. Quemener
Institut Européen des Membranes
IEM-UMR 5635
Univ Montpellier
ENSCM
CNRS
Montpellier 34090, France
E-mail: damien.quemener@umontpellier.fr

V. Bouad, D. Fournier, P. Woisel, J. Lyskawa
Univ. Lille
CNRS
INRAe
Centrale Lille
UMR 8207 – UMET – Unité Matériaux et Transformations
Lille 59000, France

F. Lefèbvre, K. Sénéchal-David, J.-N. Rebilly, F. Banse
Institut de Chimie Moléculaire et des Matériaux d'Orsay
Université Paris-Saclay
CNRS
Orsay 91400, France

The ORCID identification number(s) for the author(s) of this article can be found under https://doi.org/10.1002/admi.202300346

© 2023 The Authors. Advanced Materials Interfaces published by Wiley-VCH GmbH. This is an open access article under the terms of the Creative Commons Attribution License, which permits use, distribution and reproduction in any medium, provided the original work is properly cited.

DOI: 10.1002/admi.202300346

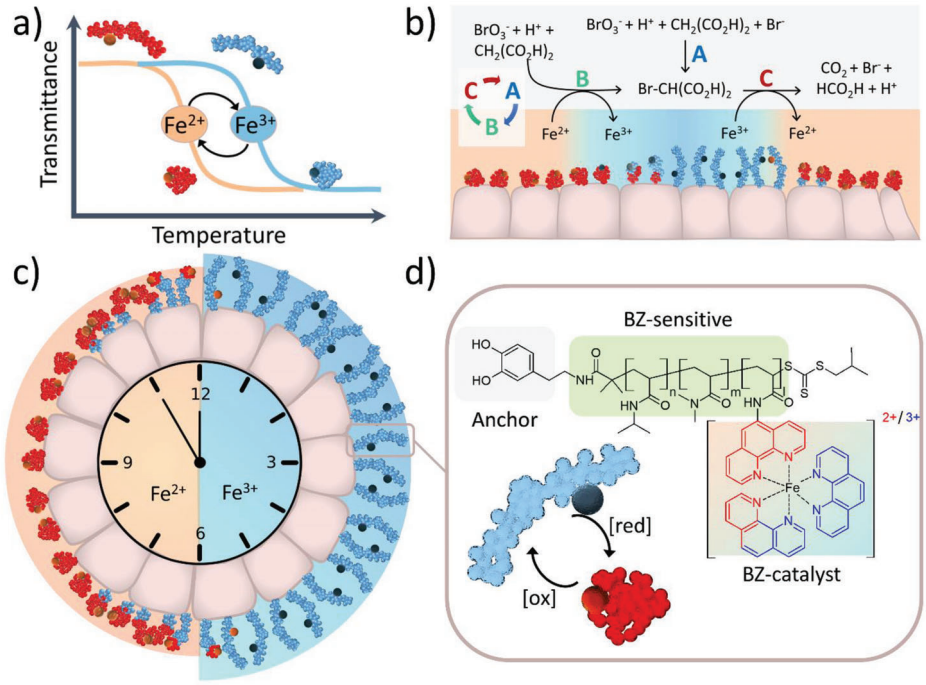

Figure 1. Schematic representation of the operation of dynamic self-oscillating materials. a) Illustration of the change in LCST as a function of the oxidation state of the polymer, monitored by measuring the transmittance of the solutions. b) Interconnections between the chemical reaction network of the BZ oscillator and a self-oscillating polymer grafted onto a surface. c) Diagram of the conformational evolution of the polymers during a redox oscillation cycle. d) Chemical structure of the BZ-sensitive self-oscillating copolymer.

32 °C in aqueous solutions.[16] PNIPAM's unique temperature-responsive behavior makes it an ideal material for biomedical applications, where it can be used to trigger morphological transitions with a simple temperature switch.[17] However, in applications that require repeated changes of polymer solubility, or where the material has a long service life, the temperature modulation cycles lead to excessive energy consumption and could cause the material to age more quickly.

To overcome this limitation, researchers have reported the use of these thermosensitive materials at a constant working temperature. For example, CO_2-switchable poly(*N*,*N*-dimethylaminoethyl methacrylate) polymers have been reported to modulate the LCST value below and above the working temperature, leading to a reversible change of the polymer conformation at a constant temperature.[18] Similarly, an LCST-like organometallic poly(ionic liquid) with a redox-sensitive poly(ferrocenylsilane) backbone has been described, where the LCST of the polymer could be changed by oxidation and reduction of the ferrocene units.[19]

The objective is to achieve greater autonomy in materials, which would allow for greater control over their life cycle, such as extending their lifespan. The use of chemical oscillators in materials science has recently been seen as another step toward full autonomy. A chemical oscillator is a network of interconnected chemical reactions that work together to achieve a periodic evolution of the composition of the medium. It can therefore autonomously modulate a stimulus such as pH.[20,21] A self-oscillating material could then be achieved if the stimulus oscillates autonomously in close proximity to a material that responds to it.

Early studies by Belousov[22] and Zhabotinsky[23,24] elucidated the periodic kinetics of oxidation reactions, known as the Belousov-Zhabotinsky (BZ) reaction, which serves as a fundamental basis for understanding the dynamics of nonlinear chemical systems. In its "traditional" form, the BZ reaction involves the oxidation of an organic substrate, such as malonic acid, under acidic conditions in the presence of an organometallic catalyst like the redox pairs Ce(IV)/Ce(III) or ferroin/ferriin. When the BZ catalyst is integrated into the backbone of a Lower Critical Solution Temperature (LCST) polymer, its oxidation leads to increased hydrophilicity, raising the LCST value. Conversely, reduction of the catalyst enhances the polymer's hydrophobicity, resulting in a lower LCST value (**Figure 1**a). These BZ-responsive organometallic polymers undergo continuous and periodic conformational switches, transitioning from coil to globule, and altering between hydrophilic and hydrophobic states when synchronized with a BZ oscillator (Figure 1b,c).

The influence of polymers on nonlinear dynamics, including oscillations, waves, patterns, and chaos, has been extensively explored.[25–26] For instance, a noteworthy observation was a periodic polymerization of acrylonitrile when coupled to a cerium-catalyzed BZ reaction.[27–28] Additionally, researchers have delved into chemomechanical instabilities in polymer gels, revealing fascinating phenomena such as spontaneous deformations and wave patterns driven by chemomechanical instabilities in responsive gels.[29–31] Furthermore, investigations into the temporal control of gelation and polymerization fronts driven by an autocatalytic enzyme reaction have demonstrated the ability to manipulate gelation and polymerization processes through precise control of the enzymatic reaction.[32]

© 2023 The Authors. Advanced Materials Interfaces published by Wiley-VCH GmbH

21967350, 0, Downloaded from https://onlinelibrary.wiley.com/doi/10.1002/admi.202300346 by Cochrane France, Wiley Online Library on [05/09/2023]. See the Terms and Conditions (https://onlinelibrary.wiley.com/terms-and-conditions) on Wiley Online Library for rules of use; OA articles are governed by the applicable Creative Commons License

A significant amount of research has been conducted on the use of LCST polymers that undergo conformational changes due to modulation of the LCST. Yoshida group has been using oscillations caused by a redox change of a ruthenium-based BZ catalyst ($[Ru(bpy)_3]^{2+} \leftrightarrow [Ru(bpy)_3]^{3+}$), which belongs to the polymer skeleton[33–35] to develop a wide range of self-oscillating materials with different functions.[36–41] However, the use of Ru-based polymers is expensive due to the scarcity of this specific metal. Therefore, it has been investigated whether iron could replace ruthenium. By adjusting the redox states of the Fe-based polymer, an LCST switch was observed, and the copolymer undergoes soluble-insoluble self-oscillation driven by the BZ reaction.[42,43] In this work published by Hara et al., NIPAM was copolymerized with 4-vinyl-4′-methyl-2,2′-bipyridinebis-(2,2′-bipyridine)-bis-(hexafluorophosphate)-iron (poly(NIPAAM-co-[$Fe(bpy)_3$])). However, LCST difference between the reduced and oxidized states of the polymer was found to be much smaller than for the comparable poly(NIPAAm-co-[$Ru(bpy)_3$]) and the resulting solubility difference was not significant enough to drive self-oscillations of high amplitude. Additionally, the ionic strength resulting from the BZ medium significantly reduced the LCST values, making it impossible to obtain BZ oscillations beyond 17 °C.[43] This could be a significant limitation when it comes to the development of iron-based BZ-responsive polymers for practical use. Despite this limitation, the use of iron as a substitute for ruthenium in these polymers could potentially lead to cost-effective production methods and open new opportunities for the development of self-oscillating materials with improved properties and performance.

In this work, iron-based BZ-responsive copolymer was synthesized using controlled radical polymerization techniques (Figure 1d). Specifically, Reversible Addition-Fragmentation Chain Transfer (RAFT) polymerization was employed to prepare polymers with targeted molecular weight. This approach allows for more precise control over the LCST values of the oxidized and reduced states, resulting in a more efficient conformational shift. By copolymerizing NIPAM and dimethylacrylamide (DMAc), the LCST of the copolymer was adjusted to operate over a wide range of applications. Additionally, RAFT polymerization allows for control over the structure of the chain ends. Here, a reactive catechol group was introduced at one chain end to subsequently graft the self-oscillating polymer onto other substrates, transforming an inert material into a dynamic responding system (Figure 1c). As an example, the BZ-responding Fe-copolymer was grafted onto the surface of an ultrafiltration membrane, resulting in a pulsating flux that can potentially prevent fouling.[44,45]

2. Results and Discussion

The primary objective of this research was to synthesize thermosensitive copolymers with a ferroin moiety and catechol unit at the end-chain, resulting in a cloud point temperature (T_{cp}) near room temperature. Although PNIPAM has a T_{cp} of ≈32 °C, the high ionic strength resulting from the BZ process (Figure 1b) tends to lower the T_{cp} by 10–15 °C, making it challenging to handle. To overcome this, the T_{cp} was increased by incorporating a hydrophilic comonomer such as DMAc into the polymer chain. The BZ-responsive copolymers (Figure 1d) were produced via RAFT polymerization, which offers the benefits of targeted molecular weights, and good control over the polymer structure. The copolymerization of NIPAAm, DMAc, and the ferroin monomer was conducted in DMF using 2,2′-azobisisobutyronitrile (AIBN) as initiator and Dopa-CTA as a chain transfer agent (Scheme S1, Supporting Information). Several copolymers with different DMAc molar ratios were synthesized (data not shown), and an 80/20 NIPAM/DMAC ratio provides the optimal T_{cp} of ≈40 °C, resulting in BZ oscillations near room temperature.

The ^{1}H NMR spectrum (Figure S6, Supporting Information) of the BZ-responsive copolymer confirms the presence of the catechol chain end, as its distinctive resonances were seen in the range of 6.5 to 6.75 ppm. The aromatic protons of the ferroin unit were detected at 8.25 to 9 ppm, and the characteristic protons of NIPAM and DMAc subunits were identified at 3.8 (N—C<u>H</u>) and 2.75 ppm (N—CH_3), respectively. By considering the integration of the protons from Dopa-CTA, ferroin, and the repeating units NIPAM and DMAc, the molecular weight of the polymer was calculated to be $\overline{M_{n\,NMR}}$ = 14 100 g mol^{-1} with the following structure: P($NIPAAM_{95}$-co-$DMAc_{26}$-co-($Fe(Phen)_3)_1$)-DOPA. Based on the chain length of the copolymer, it is possible to estimate the magnitude of the size change that occurs during the transition from a random coil to a globular conformation. To determine this, we compared the theoretical value of the copolymer's hydrodynamic radius in a good solvent medium (R_H = 8.9 nm) to the value obtained under θ conditions ($R_{H,\theta}$ = 5.2 nm) (Supporting Information). The resulting expansion factor of 1.41 for the hydrodynamic radius is substantial and should result in a significant change in the surface properties of functionalized materials under oscillations.

The cloud point of the copolymer is initially studied by monitoring the evolution of the transmittance of an aqueous solution of the copolymer in oxidized and reduced states (**Figure 2**a). As previously mentioned, the cloud point value (T_{cp}) is modulated by the oxidation state of the iron. When the complex is oxidized (Fe^{III}), the polymer becomes more hydrophilic and exhibits a T_{cp} value of ≈41.5 °C (measured at 50% transmittance). Conversely, in its reduced form (Fe^{II}), the T_{cp} value drops to 35 °C due to its more hydrophobic nature. Despite the small amount of organometallic complex in the copolymer structure (≈1 Fe per chain), the cloud point varies significantly with a six-degree difference. The autonomous oscillation of the copolymer between an insoluble hydrophobic state ($T > T_{cp,red}$) and a soluble hydrophilic state ($T < T_{cp,ox}$) can only be observed over a working temperature range $\Delta T_{cp} = T_{cp,ox} - T_{cp,red}$ (Figure 1a). Therefore, a ΔT_{cp} of 6 °C provides a comfortable margin for implementing this strategy. As expected, by controlling the architecture of the copolymers through controlled radical polymerization, we were able to surpass the results previously reported for a copolymer based on an Fe complex (ΔT_{cp} = 1.5 °C) prepared by free radical polymerization.[42] These results are also similar to those observed with ruthenium,[46] indicating a potentially large amplitude in the conformational change of the polymer. During the redox oscillations of the catalyst, the significant variation of the cloud point allows full entry into the monophasic (oxidized state) and biphasic (reduced state) domains, leading to a complete and reversible transition of the conformation of the copolymer.

The copolymer in its reduced form exhibits a distinct red-orange coloration, as evidenced by an absorbance peak at 516 nm

© 2023 The Authors. Advanced Materials Interfaces published by Wiley-VCH GmbH

21967350, 0, Downloaded from https://onlinelibrary.wiley.com/doi/10.1002/admi.202300346 by Cochrane France, Wiley Online Library on [05/09/2023]. See the Terms and Conditions (https://onlinelibrary.wiley.com/terms-and-conditions) on Wiley Online Library for rules of use; OA articles are governed by the applicable Creative Commons License

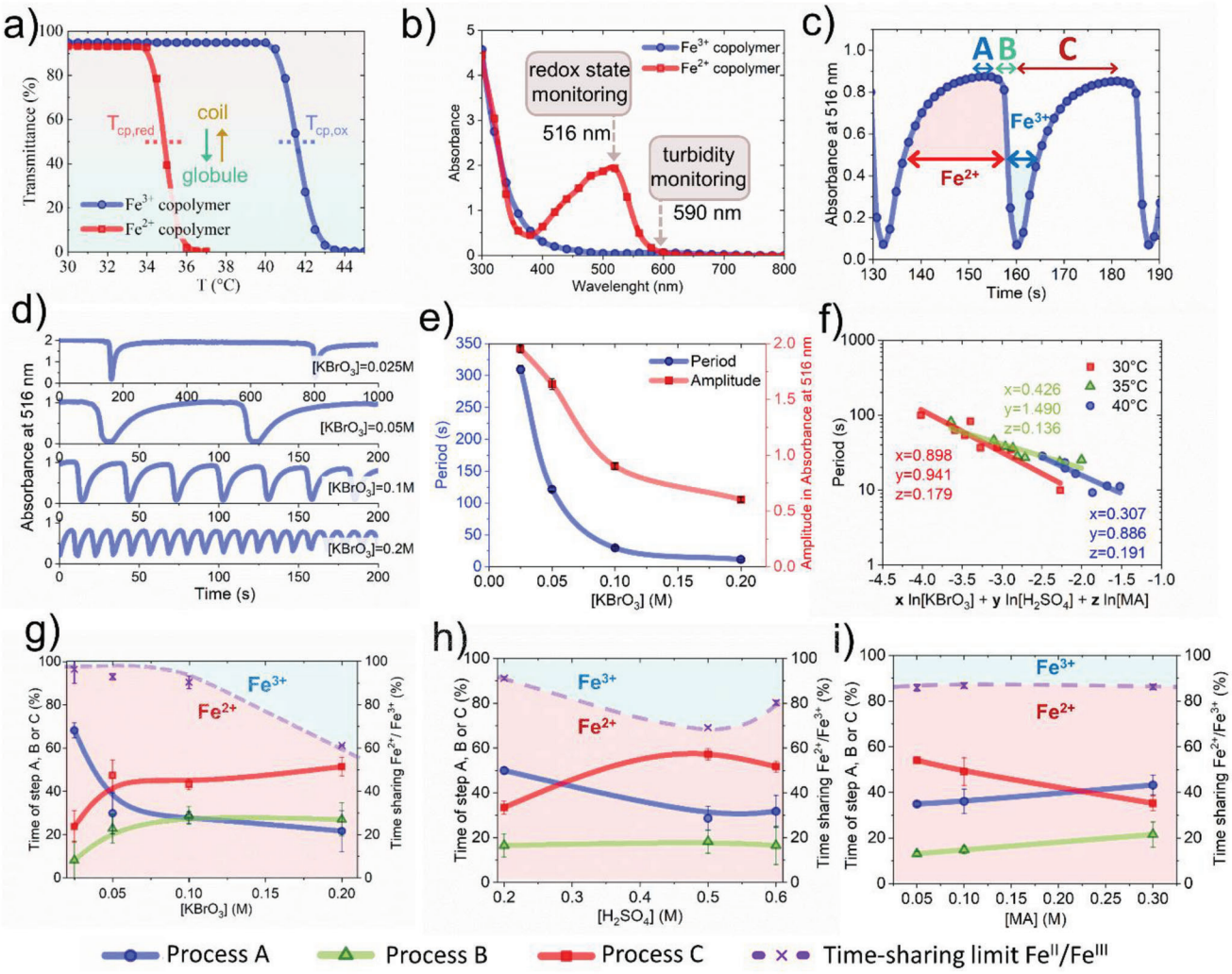

Figure 2. Characterization of copolymer oscillations in solution ([P(NIPAAM$_{95}$-co-DMAc$_{26}$-co-(Fe(Phen)$_3$)$_1$)-DOPA] = 3 mg mL^{-1}). a) Transmittance of an aqueous polymer solution as a function of temperature, continuously increased at 0.5 °C min^{-1}, in oxidized or reduced forms. b) Absorbance of copolymer solutions, in oxidized or reduced forms. c) Phases of a redox cycle of an oscillation, as shown by monitoring the absorbance at 516 nm of a BZ oscillation reaction. d) Absorbance at 516 nm of oscillation reactions at different concentrations of $KBrO_3$ at 30 °C with [MA] = 0.15 M, [H_2SO_4] = 0.35 M. e) Evolution of period and amplitude of oscillations at different concentrations of $KBrO_3$ at 30 °C with [MA] = 0.15 M, [H_2SO_4] = 0.35 M. f) Correlation between oscillation period at λ = 516 nm and reactant concentrations for different temperatures. g–i) Time sharing between the phases of the BZ oscillator (A, B, or C) and oxidation state of the copolymer, as a function of [$KBrO_3$] g) ([MA] = 0.15 M, [H_2SO_4] = 0.35 M), [H_2SO_4] h) ([MA] = 0.15 M, [$KBrO_3$] = 0.1 M), and [MA] i) ([H_2SO_4] = 0.35 M, [$KBrO_3$] = 0.1 M).

(Figure 2b). This coloration disappears in the light blue oxidized form. Additionally, there are two isosbestic points at 386 nm and 590 nm. As a result, the redox changes of the metal can be easily monitored by observing the absorbance at 516 nm, while changes in turbidity, which are solely a result of polymer precipitation in the reduced form, can be monitored at 590 nm.

The iron complex integrated into the polymer structure catalyzes an oscillatory Belousov-Zhabotinsky (BZ) reaction (Figure 1b). In this study, malonic acid is oxidized by potassium bromate in an acidic environment (H_2SO_4) and catalyzed by P(NIPAAM$_{95}$-co-DMAc$_{26}$-co-(Fe(Phen)$_3$)$_1$)-DOPA copolymer. The oscillator can be simplified as a periodic sequence of three successive processes (Figures 1b and 2c). The initial process (A) involves the consumption of Br^-, which functions as an inhibitor of the reaction, during which the catalyst is inactive and the absorbance at 516 nm remains unchanged. The second process (B), in contrast, leads to the oxidation of the complex resulting in a decrease in absorbance at 516 nm. The final process (C) resets the cycle by reducing the complex, resulting in an increase in absorbance at 516 nm. It's worth noting that these redox oscillations are accompanied by oscillations in the conformation and solubility of the polymer, which will be further analyzed.

The optimization of the concentration of the BZ oscillator components is crucial in order to achieve the desired amplitude and frequency of the redox oscillations. Figure 2d illustrates the impact of varying the bromate concentration on the redox oscillations observed at 516 nm. As the bromate concentration increases from 0.025 to 0.2 M, the amplitude of the os-

© 2023 The Authors. Advanced Materials Interfaces published by Wiley-VCH GmbH

21967350, 0, Downloaded from https://onlinelibrary.wiley.com/doi/10.1002/admi.202300346 by Cochrane France, Wiley Online Library on [05/09/2023]. See the Terms and Conditions (https://onlinelibrary.wiley.com/terms-and-conditions) on Wiley Online Library for rules of use; OA articles are governed by the applicable Creative Commons License

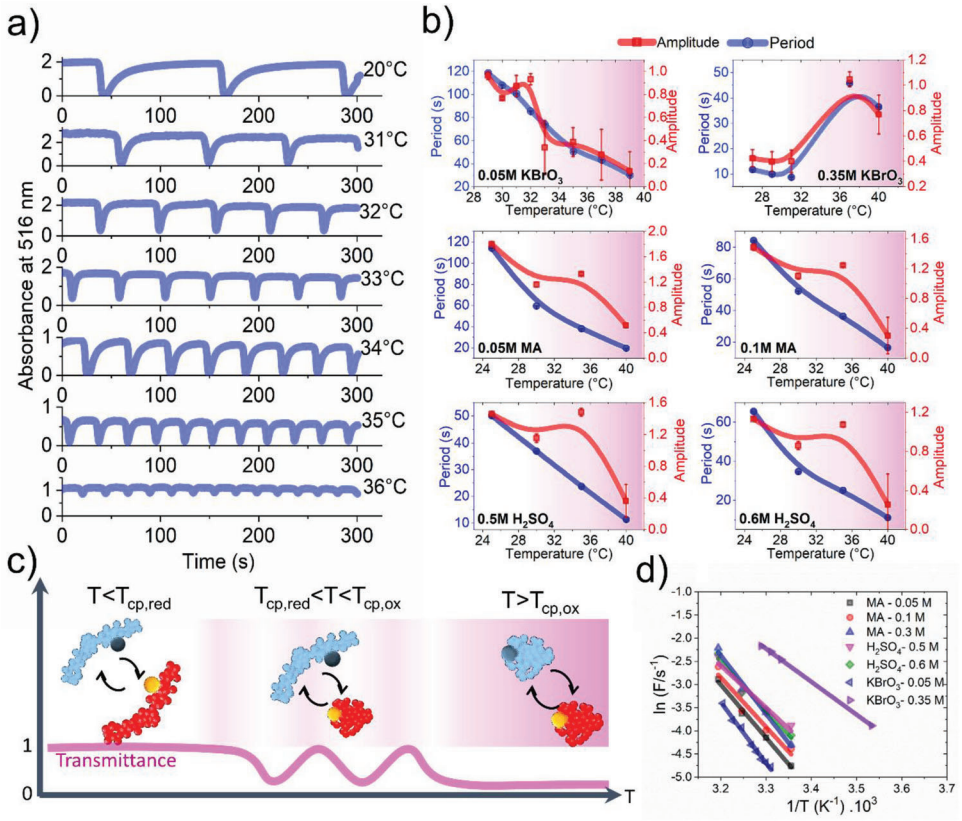

Figure 3. Influence of temperature on copolymer redox oscillations in solution. Unless otherwise stated, [MA] = 0.15 M, [H_2SO_4] = 0.35 M, [$KBrO_3$] = 0.1 M, [P(NIPAAM$_{95}$-co-DMAc$_{26}$-co-(Fe(Phen)$_3$)$_1$)-DOPA] = 3 mg mL^{-1}. a) Absorbance at 516 nm of oscillation reactions at various temperatures. b) Changes in period and amplitude of oscillations as a function of temperature. c) Schematic illustration of a temperature range for observing copolymer conformational and redox oscillations. d) Arrhenius plot showing the temperature dependence of oscillation frequency for different BZ substrate concentrations.

cillations, defined as the largest difference in absorbance during an oscillation, decreases by 68% (Figure 2e). However, the frequency of the oscillations increases with bromate concentration, with the period decreasing from 309 to 11 s. This trade-off between amplitude and frequency must be considered when trying to optimize the performance of the self-oscillating material. The period of oscillation can also be described using a power law ($P = \alpha[KBrO_3]^x[H_2SO_4]^y[MA]^z$), as seen in Figure 2f, with the concentration dependence of the oscillator components being represented by the prefactors in the empirical equations. It was found that the dependence on sulfuric acid and potassium bromate is greater than that of malonic acid, which is consistent with previous literature.[47] Additionally, the relative dependencies change as a function of temperature, with the dependence on bromate concentration decreasing at 40 °C and becoming similar to that of malonic acid. At this temperature, the polymer, in both its oxidized and reduced forms, remains in an insoluble globular state, which hinders the diffusion of reactants to the catalyst and disrupts the oscillator. Furthermore, by analyzing the different stages of the oscillation process, it is possible to gain insights into how the concentration of each reagent influences the behavior of the copolymer. As seen in Figure 2g–i, the percentage of time spent in each stage (A, B or C) of the process varies with the concentration of potassium bromate and sulfuric acid. By manipulating these concentrations, it is possible to control the duration of the "on/off switch" characterized by the two conformations of the copolymer. This allows for the modulation of the oscillator to achieve a relative equilibrium between the two states or to lead to rapid peaks in the oxidized state.

The behavior of the BZ system in response to temperature changes was further studied in detail. As shown in **Figure 3**a, an increase in temperature leads to a decrease in both the period and amplitude of the redox oscillations. This trend is observed across all concentrations of the BZ reagents (Figure 3b) and is a result of the increased kinetics of the BZ reaction at higher temperatures.[48,49] While the changes in period and amplitude are generally consistent, a notable exception occurs at a temperature ≈35°C, where a sudden increase in amplitude is observed while the period remains relatively unchanged. This is the temperature at which the redox oscillations of the iron complex are accompanied by oscillations in the copolymer chain conformation and so its solubility, resulting in a unique behavior (Figure 3c).

The Arrhenius dependence of the oscillation frequency on temperature for different concentrations of the BZ substrates was also studied (Figure 3d). Unfortunately, due to the polymer precipitation that occurs at higher temperatures, it was not possible to measure an accurate activation energy over a large enough

© 2023 The Authors. Advanced Materials Interfaces published by Wiley-VCH GmbH

21967350, 0, Downloaded from https://onlinelibrary.wiley.com/doi/10.1002/admi.202300346 by Cochrane France, Wiley Online Library on [05/09/2023]. See the Terms and Conditions (https://onlinelibrary.wiley.com/terms-and-conditions) on Wiley Online Library for rules of use; OA articles are governed by the applicable Creative Commons License

temperature range. However, an average activation energy of 86 ± 17 kJ mol^{-1} was estimated, which is consistent with previous studies in the literature.[47] Additionally, it was found that the activation energy of the oscillator was relatively independent of the concentration of malonic acid and sulfuric acid, but was sensitive to the concentration of potassium bromate. An increase in concentration from 0.05 to 0.35 M resulted in a 46% decrease in activation energy to a value of 59 kJ mol^{-1}, similar to the values reported for the best ruthenium-based systems.[50,51]

Colored patterns can be observed when oscillatory reactions are carried out in thin layers of unstirred BZ solution (**Figure 4**a–c). Blue concentric circles, formed by a high concentration of oxidized Fe^{III} copolymers, appear on a red background of reduced Fe^{II} copolymers, creating traveling waves. The temperature of the solution plays a significant role in pattern formation. At 15 °C (Figure 4a), only redox oscillations are observed as the copolymer remains in the single-phase region ($T_{15°C}<T_{cp,red}<T_{cp,ox}$). As the temperature increases to 35 °C (Figure 4b), the red Fe^{II} copolymer becomes biphasic, causing the solution to become turbid, while the blue Fe^{III} copolymer remains soluble ($T_{cp,red}<T_{35°C}<T_{cp,ox}$). At 45 °C (Figure 4c), both copolymers are in their biphasic region, resulting in a turbid solution. When the solution is placed in a stirred cell at 35 °C, an intermediate temperature so that $T_{cp,red}<T_{35°C}<T_{cp,ox}$, color and turbidity changes can be observed. For example, a clear blue phase (Fe^{III} copolymer) periodically gives way to an opaque red phase (Fe^{II} copolymer) with a period of about 20 s (Figure 4d–e and the Video S1, Supporting Information). The results of tracking the BZ reaction in a stirred cell during a temperature scan reveal an interesting trend (Figure 4f). As the temperature increases beyond 38 °C, the conformational oscillations of the copolymer (λ = 590 nm) begin to diminish, until they ultimately disappear at ≈40 °C. This phenomenon can be attributed to the fact that at this temperature, $T_{cp,ox}$ is exceeded, which leads to the disappearance of the redox oscillations. It is believed that this is due to the formation of aggregates from precipitated polymer chains, which limits the accessibility of the catalyst to the BZ components. Additionally, it was observed that no oscillatory reactions occur below 31.5 °C. However, this temperature effect is only coincidental and is due to the presence of an induction period that is commonly observed in BZ oscillators. This induction period allows for the production of intermediate species such as Br^- in sufficient concentrations to trigger redox oscillations (Figure 1b). Furthermore, the delay between the onset of redox oscillations and the onset of conformational oscillations of the copolymer is noteworthy, even though it is not directly related to temperature. As observed in Figure 4g, at 30 °C ($T_{30°C}<T_{cp,red}<T_{cp,ox}$), the redox oscillations (λ = 516 nm) occur without conformational oscillations (λ = 590 nm). However, at 35 °C ($T_{cp,red}<T_{35°C}<T_{cp,ox}$), the conformational oscillations appear after five redox cycles (Figure 4h). This shift corresponds to the number of cycles of solubility of the copolymer necessary to observe sufficient turbidity of the aqueous solution (Figure 4i). As the soluble blue Fe^{III} copolymer is reduced, the conformation of the copolymer chains changes from a random coil to a globular shape, which also results in a change in solubility, causing the appearance of turbidity. However, measurement of this turbidity at 590 nm requires that the aggregates reach a sufficient size to be detected, which is achieved from the 5th redox cycle. The relationship between the redox change of the iron and the turbidity in the solution is illustrated in Figure 4j. As the redox cycles progress, a gradual transition in the correlation between the two phenomena can be observed. This correlation eventually stabilizes after a few cycles.

Figure 5a illustrates the different domains in terms of redox state and turbidity in this system. By comparing the relative time spent in the two redox forms of the polymer with the turbidity of the solutions under varying [H_2SO_4] conditions, we can observe a delay between the redox change and the emergence of turbidity. This delay is highlighted in this figure by the fact that the turbidity region does not correspond to the region where the copolymer is reduced, which is consistent with previous results.

To get more insight, the absorbance at 516 and 590 nm can be compared (Figure 5b). The curves exhibit distinct shapes, due to the different sources of absorbance. At 516 nm, absorbance reflects the concentration of the copolymer in its reduced form (Fe^{II}), while at 590 nm, turbidity is observed. The increase in turbidity has a different kinetics than the Fe^{II} concentration, leading to dissimilar curve shapes. Of greater importance is the time lag that occurs between the two curves, which is directly attributed to the oscillation mechanism. Previous studies, such as Yoshida's,[52] have also observed a delay in self-oscillating gels and proposed a theoretical explanation based on a chemical-mechanical interplay. As shown in Figure 5c, there is a slight but significant shift between the two curves. The beginning of a cycle corresponds to the gradual transformation of the soluble Fe^{III} copolymer into the insoluble Fe^{II} copolymer. The delay at the beginning of the cycle (d_2) may correspond to the time needed for the insoluble chains to aggregate to a sufficient size to be detected as mentioned before. Conversely, the end of a cycle corresponds to the oxidation of the Fe^{II} copolymer to Fe^{III} (d_1). The shift at this time may correspond to the time it takes for the aggregates to dissolve.

Additionally, the temperature difference between the working temperature and the cloud points of the oxidized and reduced copolymer may play a role in explaining the asymmetry observed in the shifts between the beginnings and ends of the cycles. For instance, statistical measurements on Figure 5c gives different average values for d_1 = 1.12 ± 0.52 s and d_2 = 1.61 ± 0.46 s. In that experience, the shift at the beginning of the cycle is larger than at the end of the cycle, while the experiment is performed at a temperature close to $T_{cp,red}$. However, if the experiment is conducted at a temperature close to $T_{cp,ox}$, the offset at the beginning of the cycle is smaller than at the end of the cycle. Figure 5d illustrates the discrepancy in delay. By examining the shape of the absorbance curve at 516 nm (Figure 2c), which directly measures the concentration of the reduced polymer, we can see a gradual transition. The curve for the cloud points of the oxidized copolymer in the phase diagram gradually decreases until it reaches the fully reduced form of the polymer and passes through the working temperature at which the experiment was conducted. We can understand that the relative position of the working temperature in relation to the T_{cp} of the two curves is crucial. The evolution of the mean T_{cp} value is shown in Figure 5e. It is defined as $T_{cp} = \alpha T_{cp,red}. +(1\text{-}\alpha)T_{cp,ox}$, where α is the molar fraction of polymer in the reduced state, determined from the absorbance at 516 nm. We assume that the T_{cp} value is directly proportional to the relative composition of the mixture of oxidized and reduced species, i.e., to the Fe^{II} concentration. If we position the working

© 2023 The Authors. Advanced Materials Interfaces published by Wiley-VCH GmbH

21967350, 0, Downloaded from https://onlinelibrary.wiley.com/doi/10.1002/admi.202300346 by Cochrane France, Wiley Online Library on [05/09/2023]. See the Terms and Conditions (https://onlinelibrary.wiley.com/terms-and-conditions) on Wiley Online Library for rules of use; OA articles are governed by the applicable Creative Commons License

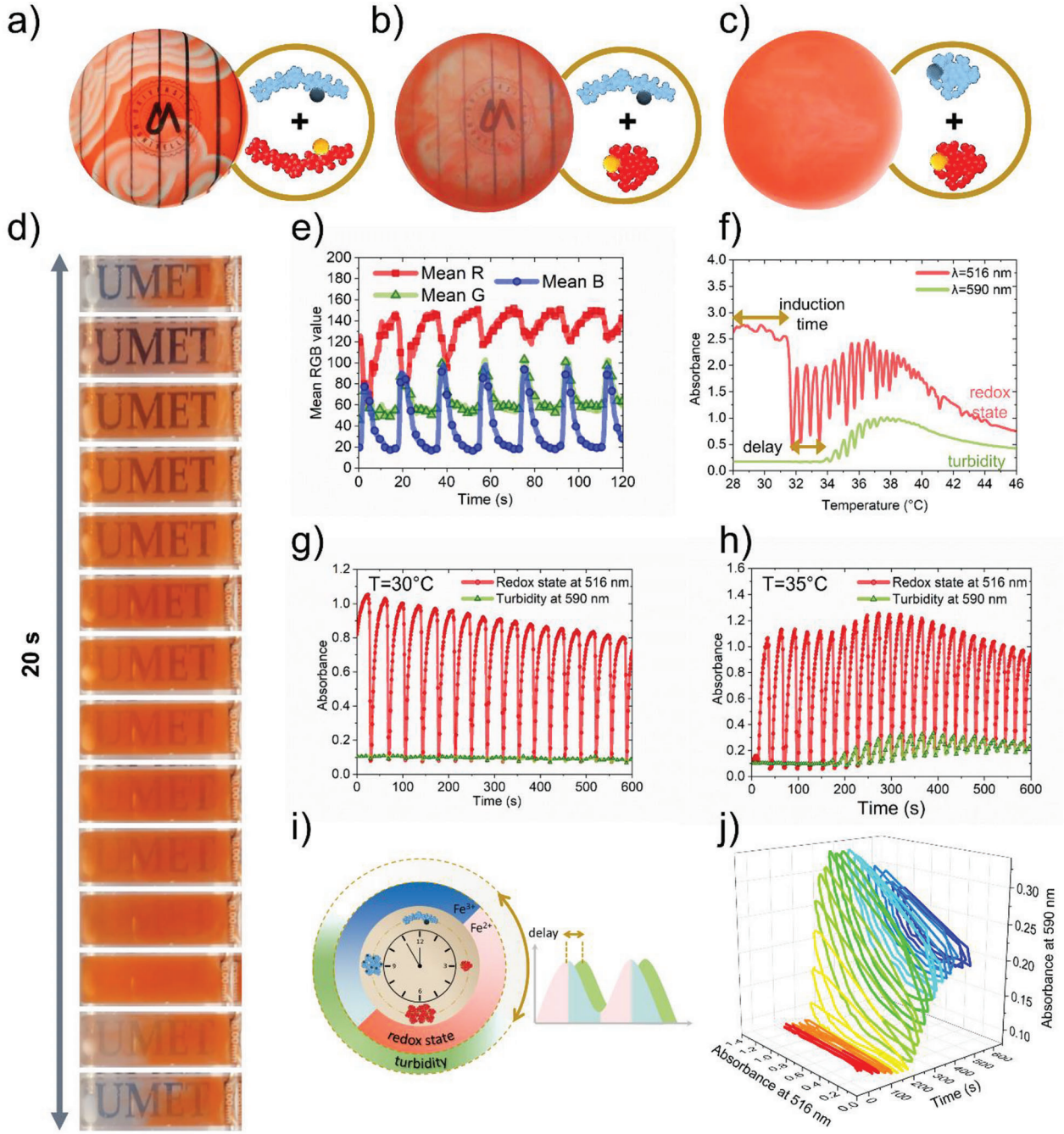

Figure 4. Conformational oscillations of the copolymer in solution. a–c) BZ oscillations in unstirred solutions of P(NIPAAM$_{95}$-co-DMAc$_{26}$-co-(Fe(Phen)$_3$)$_1$)-DOPA (3 mg mL^{-1}) at T = 15 °C (a), T = 35 °C (b), T = 45 °C (c) in a petri dish. d) Temporal evolution of one oscillation cycle of copolymer solution at 35 °C in a stirred cuvette (images rotated 90° for better readability). e) Changes in Red, Green, and Blue color values during the oscillation reaction (extracted from the Video S1, Supporting Information). f) Thermal scanning of copolymer oscillations at 1 °C min^{-1} for λ = 516 nm and λ = 590 nm. g–h) Absorbance of copolymer oscillations over time at 30 °C (g) and 35 °C (h). i) Schematic illustration of the observed time lag between redox changes and turbidity. j) 3D correlation between redox (516 nm) and conformational (590 nm) oscillations of the copolymer as a function of time.

temperature (T) closer to $T_{cp,red}$ as in our example, we observe a higher value for d_2 than for d_1. However, this explanation must be considered in light of the steep slope of the curve, which can quickly reverse the result. This time delay is a result of the interplay between the onset of measurable turbidity and the kinetics of redox reactions and their impact on copolymer conformation at a selected working temperature.

Furthermore, the ionic strength of the medium, which varies with the concentration of the components of the BZ oscillator, plays a role in the observed offsets. This effect, known in the

© 2023 The Authors. Advanced Materials Interfaces published by Wiley-VCH GmbH

21967350, 0, Downloaded from https://onlinelibrary.wiley.com/doi/10.1002/admi.202300346 by Cochrane France, Wiley Online Library on [05/09/2023]. See the Terms and Conditions (https://onlinelibrary.wiley.com/terms-and-conditions) on Wiley Online Library for rules of use; OA articles are governed by the applicable Creative Commons License

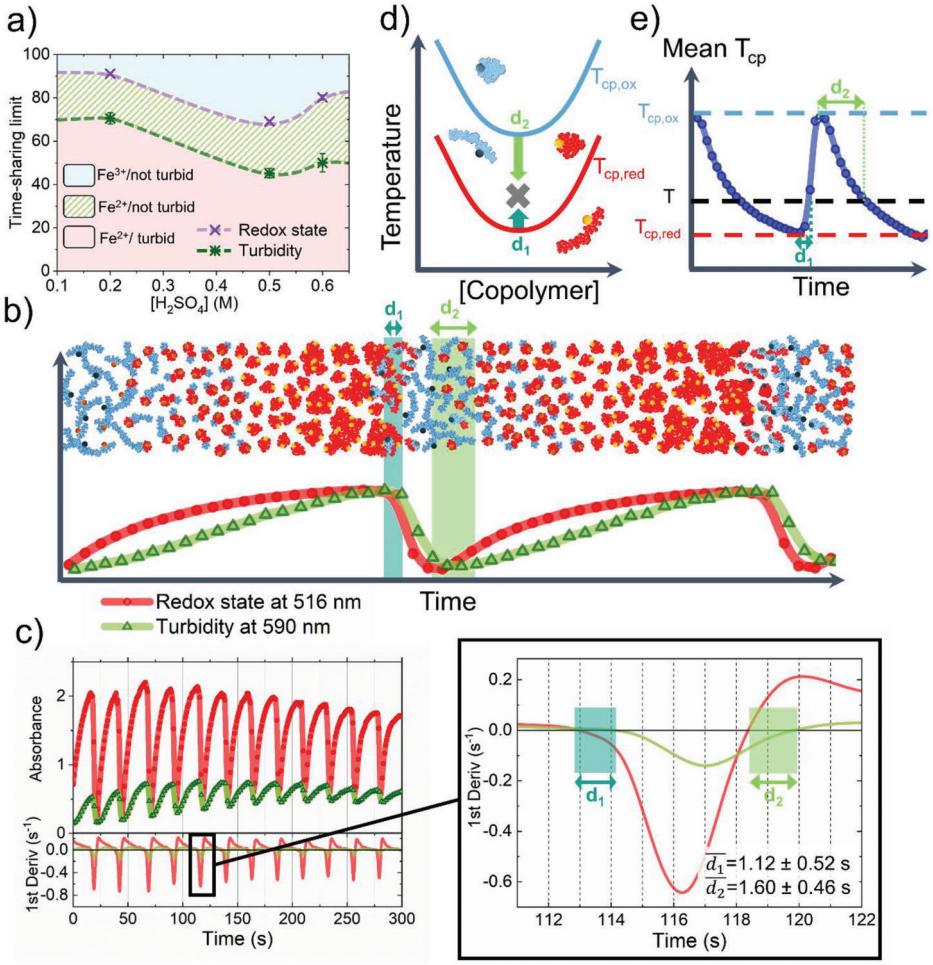

Figure 5. Investigating the time lag between redox oscillations and turbidity. a) Distribution of time between turbidity and oxidation state for various H_2SO_4 concentrations. The time limits were evaluated by analyzing the midpoint of the absorbance curves over time. The Fe^{II}/Fe^{III} threshold was established at 516 nm, while the turbidity threshold was measured at 590 nm. b) Changes in absorbance at 516 and 590 nm over time with a corresponding illustration of copolymer conformation in solution. c) Analysis of the time lag at the beginning and end of cycles (d_1, d_2) based on the first derivative of absorbance over time. $\overline{d_1}$ and $\overline{d_2}$ represent the average values of 12 cycles. d) Solution phase behavior of the LCST copolymer P(NIPAAM$_{95}$-co-DMAc$_{26}$-co-(Fe(Phen)$_3$)$_1$)-DOPA during a BZ oscillation. e) Comparison of the relative evolution of the cloud point during a redox cycle to the working temperature.

literature as the decrease of T_{cp} with increasing ionic strength,[53] is dependent on the initial concentrations of the introduced oscillator components and the fluctuation of the ionic strength during the reaction. To understand the potential impact of varying ionic strength on our analysis, we created a model of the primary reaction equations of the oscillator and simulated the oscillations under the conditions of our experiment (Supporting information). The results of the simulation revealed expected oscillations in the composition of the medium (Figure S14–S15, Supporting Information). When we used the simulation to estimate the fluctuation of the ionic strength throughout the oscillations, it was found to only vary by a small margin of 0.32% (Figure S16–S17, Supporting Information). This suggests that the fluctuation of ionic strength likely has little to no influence on the evolution of the T_{cp}.

To demonstrate the potential of self-oscillating polymers in materials science, we grafted the P(NIPAAM$_{95}$-co-DMAc$_{26}$-co-(Fe(Phen)$_3$)$_1$)-DOPA copolymer onto ultrafiltration membranes. These membranes are commonly used for virus filtration but are prone to fouling. Filtration membrane fouling is a complex phenomenon in which contaminants accumulate on the membrane surface, resulting in reduced performance and efficiency. To mitigate fouling, researchers have investigated several strategies including physical cleaning, chemical cleaning, membrane modification, and operational control. Pulsed flow is often cited as a possible solution to reduce fouling in membrane filtration systems.[44,45] The basic principle behind pulsed flow is to disrupt the formation of a continuous fouling layer on the membrane surface, which can improve performance and extend the lifespan of the membrane. The profile of conformational oscillations obtained in this work in the form of an Fe^{III} pulse in an Fe^{II} background seems relevant to obtain a pulsed flux. To this end, we grafted P(NIPAAM$_{95}$-co-DMAc$_{26}$-co-(Fe(Phen)$_3$)$_1$)-DOPA chains onto the surface of an ultrafiltration membrane via their catechol

© 2023 The Authors. Advanced Materials Interfaces published by Wiley-VCH GmbH

21967350, 0, Downloaded from https://onlinelibrary.wiley.com/doi/10.1002/admi.202300346 by Cochrane France, Wiley Online Library on [05/09/2023]. See the Terms and Conditions (https://onlinelibrary.wiley.com/terms-and-conditions) on Wiley Online Library for rules of use; OA articles are governed by the applicable Creative Commons License

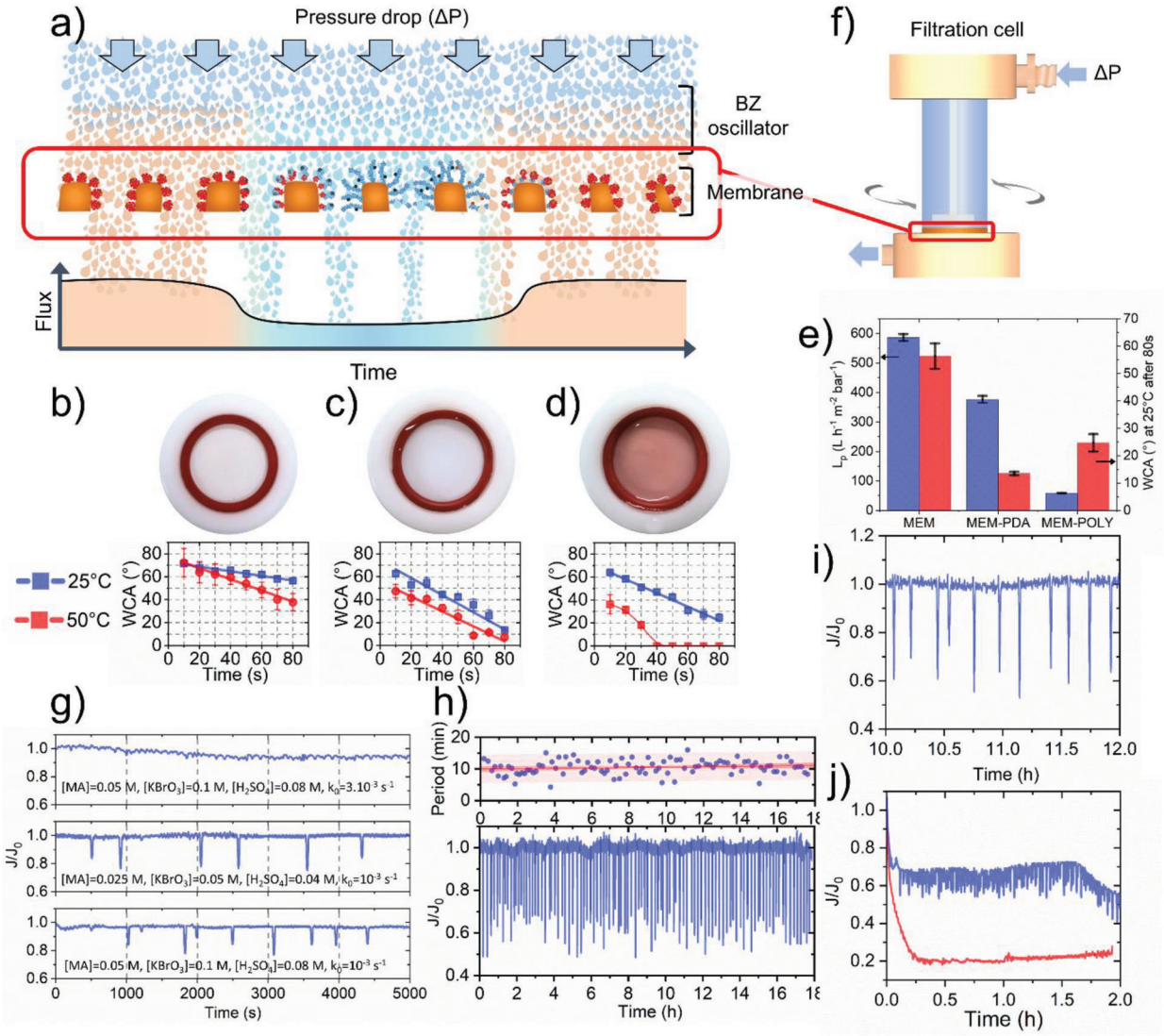

Figure 6. Self-oscillating water permeation through a functionalized ultrafiltration membrane. a) Illustration of the self-oscillating water permeation through the copolymer-functionalized membrane during one cycle of the BZ oscillation reaction. b–d) Functionalization steps of the membrane. Upper part: photo of the membrane. Lower part: evolution of the water contact angle with time at 25 and 50 °C. b) Virgin PES membrane (MEM). c) PES membrane after polydopamine deposition (MEM-PDA). d) Membrane after grafting of P(NIPAAM$_{95}$-co-DMAc$_{26}$-co-(Fe(Phen)$_3$)$_1$)-DOPA on MEM-PDA (MEM-POLY). e) Evolution of the water permeance of the membranes and the water contact angle at 25 °C after 80 s of stabilization after each functionalization step. f) Schematic diagram of a dead-end filtration cell with stirring, where water permeation occurs. g) Comparison of water permeation (flux normalized by the initial flux (ΔP = 1 bar)) through the membrane under various conditions, with different reactant concentrations and k_0 (Inverse of the residence time). h–i) Water permeation under oscillation over a long time. Concentrations in tanks: [MA] = 0.086 м, [$KBrO_3$] = 0.196 м, [H_2SO_4] = 0.168 м. Initial concentrations in the filtration cell: [MA] = 0.043 м, [NaBr] = 0.010 м, [$KBrO_3$] = 0.098 м, [H_2SO_4] = 0.084 м. k_0 = 3.01 10^{-4} s^{-1}, ΔP = 1 bar. h) Lower panel: Evolution of water flux normalized by the initial flux (ΔP = 1 bar). Upper panel: measurement of the oscillation period over time with confidence and prediction bands at 95% of a linear fitting of the data. i) Enlargement of the water permeation curve under oscillations. j) BSA filtration with (top curve, [MA] = 0.1 м, [$KBrO_3$] = 0.4 м, [H_2SO_4] = 0.17 м. k_0 = 10^{-3} s^{-1}, ΔP = 1 bar, 35 °C) and without (bottom curve, [$KBrO_3$] = 0.4 м, [H_2SO_4] = 0.17 м. k_0 = 10_{-3} s^{-1}, ΔP = 1 bar, 35°C) flow oscillations.

end. According to the Hagen-Poiseuille law, the volumetric flow rate is directly proportional to the power of four of the pore radius. Therefore, a small variation in pore size can significantly affect the flow rate value. Localized in the pores, the autonomous contraction/extension cycles of the copolymer chains could thus generate the desired pulses (**Figure 6**a).

To achieve this, we first pre-coated polyethersulfone (PES) membranes with a thin layer of polydopamine (PDA) (Scheme S2, Supporting Information). PDA intermediate layer allows easy post-functionalization of the materials without significantly changing the pore size at low deposition time (15 min).[21] PDA-functionalized membranes were then impregnated under pressure with P(NIPAAM$_{95}$-co-DMAc$_{26}$-co-(Fe(Phen)$_3$)$_1$)-DOPA solution in order to maximize an in-depth grafting. In SEM images, no alteration in PES membranes was observed after PDA deposition and after P(NIPAAM$_{95}$-co-DMAc$_{26}$-co-(Fe(Phen)$_3$)$_1$)-DOPA

© 2023 The Authors. Advanced Materials Interfaces published by Wiley-VCH GmbH

21967350, 0, Downloaded from https://onlinelibrary.wiley.com/doi/10.1002/admi.202300346 by Cochrane France, Wiley Online Library on [05/09/2023]. See the Terms and Conditions (https://onlinelibrary.wiley.com/terms-and-conditions) on Wiley Online Library for rules of use; OA articles are governed by the applicable Creative Commons License

grafting (Figure S7, Supporting Information). The grafting of the copolymer is characterized in particular in XPS by a decrease in the atomic percentage of S present in quantity in the virgin PES membrane, as well as an increase in the percentage of N present on the repeating units of the copolymer (Figure S8–S12 and Table S1, Supporting Information). Figure 6b–d shows the change in color from white to red of the membrane after the copolymer grafting, confirming the presence of $Fe(Phen)_3)_1$ moiety. The water contact angle (WCA) decreases over time after the deposition of a drop of water due to the porosity of the membranes. The evolution of WCA at two temperatures (25 and 50 °C) is linear for the pristine PES membrane (MEM) as well as for the polydopamine functionalized membrane (MEM-PDA). On the other hand, a break in linearity is observed at 50 °C when the copolymer is grafted onto MEM-PDA (MEM-POLY). Indeed, WCA drops rapidly with time to reach 0° in 40 s. This evolution is the result of the existence of a cloud point in aqueous solution. Indeed, when a drop of water at 50 °C is deposited, the copolymer chains will collapse on the pore wall and contribute to the water absorption by capillarity. The water permeance measured after each functionalization step is given in Figure 6e. Since each step contributes to reducing the pore size, it is logical to observe a decrease in permeance after polydopamine (PDA) deposition and then after copolymer grafting. Moreover, the WCA at 25 °C decreases during PDA deposition due to its hydrophilic nature. On the other hand, this angle increases slightly after grafting of the copolymer, witnessing its more hydrophobic character.

The membrane was then washed and mounted in a dead-end filtration cell (Figure 6f). When BZ water solution was passed at a too high velocity ($k_0 = 3.10^{-3}$ s^{-1}, k_0 being the inverse of the residence time) through the functionalized membrane, a stable flux was observed (Figure 6g). Here, the BZ reaction network does not have time to establish itself, thus preventing the appearance of redox oscillations and therefore flux oscillations. However, when the residence time is increasing ($k_0 = 10^{-3}$ s^{-1}), negative peaks with random periodicity appeared, causing a disturbance in the flux as desired. An intermittent relaxation of the flow such that obtained in this work was found to be highly effective for mitigate organic fouling.[44] The lack of periodicity is likely due to the open system design of the filtration process, where the BZ oscillator components remain in the filtration cell for a residence time dependent on the flux value, not to mention the Fe BZ catalyst immobilized on the membrane. We also found that by doubling the concentration of oscillator components, the number of negative peaks increased. By assuming that the pore walls were lined with copolymers, we estimated that the variation in pore size caused by the conformational change of the polymer was at most 10.4 nm for a pore diameter of ≈20 nm (Supporting Information). While this value is likely overestimated, it illustrates the potential of these self-oscillating copolymers to greatly affect the flow of a fluid through the membrane (Figure 6a).

A water permeation experiment under oscillations was then carried out over nearly 18 h in order to verify the robustness of the process (Figure 6h–i). Over this period of time, 105 peaks were detected with an average rate of flux decrease during an oscillation of 38.0±6.7%. Fourier transforms (data not shown) shows broadband amplitude spectrum typical of chaos. Even if the oscillations are not regular, the average period of oscillations is 10.52 min with an acceptable standard deviation equal to 2.37 min. After this experiment, the cell body is removed and a thin film of BZ solution is kept so that the visual appearance of the membrane can be observed over 4 min (Figure S13, Supporting Information). We can observe a random pattern showing the polymer in its two states, reduced (red) and oxidized (very light blue). The presence of a layer of BZ solution allows to maintain the oscillator reaction network on the surface of the membrane and an evolution of the pattern is visible with areas going from light blue to red and vice versa. After 2 min, the BZ solution is replaced by a thin film of pure water and the membrane rapidly evolves toward a homogeneous red, like a reset of the oscillator clock. Note also that this confirms the integrity of the copolymer functionalization after filtration under oscillation.

To investigate the impact of flow disturbances on fouling, we conducted two filtrations of bovine serum albumin (BSA), a model protein commonly used in fouling tests, under identical conditions, except for the presence or absence of malonic acid, which induces flow oscillations (Figure 6j). In the absence of malonic acid, a rapid decline of ≈80% of the initial flux was observed within 15 min, caused by the accumulation of BSA on the membrane surface. In contrast, when malonic acid was present, we observed flux oscillations that limited the decline to ≈30% of the initial flux. We speculate that the initial decline was due to the time required to establish the oscillation regime in the filtration cell. Once established, the flux remained stable. However, after 1.5 h of filtration, a decrease in flux was observed, indicating the gradual accumulation of BSA on the membrane surface. Beyond a critical BSA concentration, flux oscillations could no longer prevent fouling. Further research is required to fully understand the factors contributing to fouling.

The use of self-oscillating polymers in materials science has the potential to revolutionize the field. The ability to modulate the properties of materials dynamically, in response to changes in the environment, opens up a wide range of possibilities for new and improved applications. For example, the ability to generate rapid negative flux peaks in ultrafiltration membranes can disrupt the flux and adhesion of fouling species, making the membranes more efficient and longer lasting. This has the potential to improve filtration processes across a wide range of industries, including water treatment, biotechnology, and pharmaceuticals. Furthermore, the ability to modulate the properties of materials dynamically can also be applied to other areas such as energy storage, sensing, and actuators. One avenue of improvement would be to further optimize the polymer synthesis process to achieve a higher level of control over the oscillation period and amplitude. Additionally, research could be done to explore the use of different types of catalysts and monomers in polymer synthesis to create a wider range of self-oscillating polymers with different properties. Another area of exploration would be to investigate the use of these polymers in other types of applications beyond membrane filtration, such as in smart coatings or self-healing materials. Overall, this research represents a promising step toward the development of autonomous materials that can dynamically respond to their environment.

3. Conclusion

In this work, we developed a terpolymer of *N*-isopropylacrylamide, dimethylacrylamide, and an iron-based

© 2023 The Authors. Advanced Materials Interfaces published by Wiley-VCH GmbH

21967350, 0, Downloaded from https://onlinelibrary.wiley.com/doi/10.1002/admi.202300346 by Cochrane France, Wiley Online Library on [05/09/2023]. See the Terms and Conditions (https://onlinelibrary.wiley.com/terms-and-conditions) on Wiley Online Library for rules of use; OA articles are governed by the applicable Creative Commons License

BZ comonomer by using RAFT polymerization. The ratio of NIPAM and DMAc was carefully selected to achieve an oscillating working temperature of 35 °C. Additionally, we introduced a catechol unit as part of the initial RAFT agent at the end of the copolymer chains to enable subsequent grafting of the copolymer onto a variety of substrates. Through investigating the redox oscillations, we were able to determine the optimal range of BZ reagent concentrations for maximizing the oscillation amplitude and frequency. By operating at a temperature between $T_{cp,red}$ and $T_{cp,ox}$, we were able to observe the conformational oscillation of the polymer as a direct result of the redox oscillations. This study has shown the potential of using self-oscillating polymers in materials science, specifically in the field of filtration. By grafting the Fe-based copolymer onto an ultrafiltration membrane, the material is able to continuously modulate the size of the pores through autonomous expansion and contraction cycles. This results in rapid negative flux peaks that disrupt the flux and the adhesion of fouling species to the membrane. The results of this study demonstrate the ability of these self-oscillating polymers to make inert materials dynamic and give them new properties. The interplay of chemical reactions and mechanical response is a new step toward autonomous materials that can react to their environment. This research opens up new possibilities for the development of intelligent materials with self-regulating properties that can adapt to changing conditions.

4. Experimental Section

Materials: All reagents were purchased from Sigma–Aldrich and used without further preparation unless otherwise stated. *N*-isopropylacrylamide (NIPAM) and 2,2′-azobis(isobutyronitrile) (AIBN) were recrystallized from hexane and methanol, respectively. Dimethylacrylamide (DMAc) was purified over silica to remove inhibitor. Dimethylformamide (DMF) was distilled over calcium hydride and stored under nitrogen atmosphere before use. Sodium sulfate, sodium chloride, sodium bromide, hexane, acetone, ethanol, and diethyl ether were purchased from VWR and used as received. Dopa-CTA was synthesized according to the procedure described in the literature.[54] 1,10-phenanthrolin-5-yl-acrylamide was synthesized according to literature.[55] Commercial polyethersulfone membranes with MWCO = 100 kDa, 63.5 mm diameter (Millipore®, PBHK06210) were washed for 1 h by immersion in MilliQ water, changing the water three times before use.

Characterizations: ^{1}H NMR spectra were recorded at 25 °C using either a Bruker Avance 300 spectrometer (Polymer) or a Bruker 360 MHz spectrometers (Monomer). Deuterated water (D_2O) and dimethylsulfoxide (DMSO-d^6) were used as solvents, and chemical shifts were expressed in ppm with respect to tetramethylsilane (TMS). UV–vis measurements were performed using Agilent Cary 3500 UV–vis spectrometer equipped with a temperature controller. UV–vis spectra were recorded at 20 °C. A polymer concentration of 0.5 mM was used for the cloud point measurements. Transmittance was recorded at 750 nm with a cooling/heating rate of 1°C min^{-1} and the cloud point were determined at the beginning of the abrupt decrease in transmittance. ESI mass spectrometry analyses were performed with a Bruker MicroTOFq spectrometer using a sodium formate calibrant. Cyclic Voltammetry experiments were performed using an Autolab potentiostat and a conventional three electrodes device (C working electrode, SCE reference electrode, Pt counter electrode). The electrolyte salt ($TBAPF_6$) was recrystallized and all the glassware was dried at 110 °C before use. All the cyclic voltammograms (CVs) were recorded under argon in acetonitrile solution containing 0.1 M Bu_4NPF_6 at a scan rate of 0.1 V s^{-1} at 20 °C. All potential values are referred to SCE. Thermogravimetric analyses (TGA) were performed under air flow from room temperature up to 800 °C using a TA Instruments SDT Q600 apparatus.

Synthesis of [(phen)$_2$(phen-5-yl-acrylamide)Fe^{II}](PF$_6$)$_2$: From 0.7 M stock solutions of phen and phen-5-yl-acrylamide in CH_2Cl_2, a 2:1 mixture of phen: phen-5-yl-acrylamide (12 mL/6 mL) was made. The solution was evaporated to dryness and the stoichiometry was controlled by ^{1}H NMR in D^6-DMSO. In a schlenk tube, $FeSO_4.7H_2O$ (1.357 g, 4.88 mmol) was dissolved in 5 mL water, and degassed under argon. The previous mixture of phen (9.76 mmol) and phen-5-yl-acrylamide (4.88 mmol) was added as a solid, and the dark red solution was stirred overnight under argon. NH_4PF_6 (1.591 g, 9.76 mmol) in water (5 mL) was added leading to the precipitation of the complex. The mixture was stirred for 20 min before filtering the complex. The solid was washed with cold water (3×5 mL) and diethyl ether (3×5 mL) and dried under vacuum (3.6 g, 73%). ^{1}H NMR (CD_3CN, 360 MHz, 300 K) δ (ppm): 9.01 (s, 1H, (C = O)NH), 8.73 (m, 2H, H_{arom}), 8.61 (m, 4H, H_{arom}), 8.56 (dd, J = 7.9 Hz, J' = 1.6 Hz, 1H, H_{arom}), 8.26 (s, 4H, H_{arom}), 7.62 (m, 12H, H_{arom}), 7.62 (m, 12H, H_{arom}), 6.67 (dd, J = 17 Hz, J' = 11 Hz, 1 H, $H_{acrylamide}$), 6.48 (dd, J = 17 Hz, J'' = 1.6 Hz, 1 H, $H_{acrylamide}$), 5.92 (dd, J' = 11 Hz, J'' = 1.6 Hz, 1 H, $H_{acrylamide}$). ESI-MS: m/z = 332.5801 (calcd for [(phen)$_2$(phen*)Fe]$^{2+}$ 332.5813, error = 3.6 ppm). Phen stands for 1,10-phenanthroline and phen* for 1,10-phenanthrolin-5-yl-acrylamide. Electrochemistry: reversible Fe$^{III/II}$ couple at $E_{1/2}$ = 1.1 V (ΔE = 100 mV) versus SCE. UV–vis (MeCN, 300 K): λ_{max} = 435 nm (MLCT, ϵ = 14 400 L mol^{-1} cm^{-1}) and λ_{max} = 510 nm (MLCT, ϵ = 17 500 L mol^{-1} cm^{-1}), λ_{max} = 265 nm (π- π*, ϵ = 124 000 L mol^{-1} cm^{-1}) (Figures S1–S5, Supporting Information).

Synthesis of P(NIPAAM-co-DMAC-co-Fe(Phen)$_3$)-DOPA: In a Schlenk tube, NIPAM (1.3 g, 0.0115 mol), DMAC (0.613 g, 0.0062 mol), [(phen)$_2$(phen-5-yl-acrylamide)Fe^{II}](PF$_6$)$_2$ (0.919 g, 9.2×10^{-4} mol), AIBN (12.4 mg, 7.5×10^{-5} mol) and the chain transfer agent (CTA-DOPA, 98 mg, 2.5×10^{-4} mol) were added in dry DMF (5 mL). The mixture was deoxygenated by argon bubbling for 30 min and then heated to 80 °C for 2 h. The polymer was purified by dialysis against ethanol for 20 days using 1 kDa porous membranes. After dialysis, the solution was evaporated and dried to constant weight. The polymer was resolubilized in DI water and the insoluble part was removed by centrifugation. The supernatant solution was then freeze-dried to obtain the BZ-responding copolymer. P(NIPAAM$_{95}$-co-DMAC$_{26}$-co-(Fe(Phen)$_3$)$_1$)-DOPA, $\overline{M_n}_{NMR}$ = 14 100 g mol^{-1}.

Functionalization of Membrane with BZ-Responsive Copolymer: To functionalize the PES commercial membranes with a BZ-responsive copolymer, a polydopamine (PDA) intermediate layer was coated onto the membranes following a procedure adapted from literature.[56] Three 24 mm diameter membranes were cut from the 64 mm commercial membrane and washed in Milli-Q water for 1 h. A pH 8.5 solution was prepared using a 10:1 ratio of Milli-Q water and tris glycine buffer, to which dopamine was added to a concentration of 0.1 mg mL^{-1}. The membranes were then immersed in the dopamine solution under stirring (70 rpm) for 15 min. After the reaction was complete, the membranes were washed with Milli-Q water, subjected to an ultrasound bath for 15 min, and stored in a 95:5 (v:v) Milli-Q water and ethanol mixture. A solution of P(NIPAAM$_{95}$-co-DMAC$_{26}$-co-(Fe(Phen)$_3$)$_1$)-DOPA was prepared in Milli-Q water at pH 8.5. The PDA-coated PES membrane was placed in the solution and the reaction was carried out at 55 °C for 2 h. After the reaction was complete, the membrane was rinsed with Milli-Q water, subjected to an ultrasound bath for 15 min, and then stored in a 95:5 (v:v) Milli-Q water and ethanol mixture.

Measurement of Cloud Point (Tcp): The transmittance of the copolymer was measured in its reduced state using an acidic solution containing P(NIPAAM$_{95}$-co-DMAC$_{26}$-co-(Fe(Phen)$_3$)$_1$)-DOPA (10^{-3} M) and H_2SO_4 (0.3 M). The transmittance was measured in its oxidized state using a mixture of H_2SO_4 (0.3 M), $KBrO_3$ (0.1 M), and copolymer (10^{-3} M) with a temperature ramp from 15 to 45°C at a rate of 0.5°C min^{-1}, with a one-minute temperature stabilization time between each measure.

Isobestic Point Measurement: A solution of P(NIPAAM$_{95}$-co-DMAC$_{26}$-co-(Fe(Phen)$_3$)$_1$)-DOPA (10^{-3} M), H_2SO_4 (0.3 M), and $KBrO_3$ (0.1 M) was prepared and immediately analyzed using UV–vis spectroscopy after observing the change in color of the solution, which indicated the change in oxidation state of the catalyst. The spectrum was compared with that of a solution of P(NIPAAM$_{95}$-co-DMAC$_{26}$-co-(Fe(Phen)$_3$)$_1$)-DOPA (10^{-3} M) and H_2SO_4 (0.3 M), which corresponds to the reduced state of the catalyst.

© 2023 The Authors. Advanced Materials Interfaces published by Wiley-VCH GmbH

21967350, 0, Downloaded from https://onlinelibrary.wiley.com/doi/10.1002/admi.202300346 by Cochrane France, Wiley Online Library on [05/09/2023]. See the Terms and Conditions (https://onlinelibrary.wiley.com/terms-and-conditions) on Wiley Online Library for rules of use; OA articles are governed by the applicable Creative Commons License

Measuring Water Permeation under BZ Oscillations: A 24 mm diameter membrane was placed in a 14 ml stainless steel dead-end filtration cell. The cell was connected to a 1L Amicon tank filled with Milli-Q water, allowing for adjustable pressure. Permeated water was measured using a balance and recorded by the S232 Data Logger software with a 0.599 s time interval acquisition. Prior to measuring permeability, a conditioning step was applied by applying a pressure drop of 4 bar for 30 min. To measure water permeation under BZ oscillations, aqueous feed solutions were premixed in two tanks and entered the dead-end filtration cell at the same flow rate (Tank 1: $KBrO_3$ and H_2SO_4; Tank 2: MA). The BZ oscillator was set up in the filtration cell under pressure and with a targeted k_0 value, which corresponds to the inverse of the residence time in the filtration cell. During filtration experiments, BSA was added in the Tank 2 together (with oscillations) or instead (without oscillations) of malonic acid.

Supporting Information

Supporting Information is available from the Wiley Online Library or from the author.

Acknowledgements

The authors thank the Institut Universitaire de France (IUF) and the Agence Nationale de la Recherche (ANR) through the OsciMEM project (ANR-20-CE06-0013-01) for financial support. Didier Cot and Maxime Ruiz were acknowledged, respectively for SEM analysis and longtime water permeance under oscillations.

Conflict of Interest

The authors declare no conflict of interest.

Data Availability Statement

The data that support the findings of this study are available from the corresponding author upon reasonable request.

Keywords

Belousov-Zhabotinsky oscillator, membrane, self-oscillating polymer, stimuli-responsive polymer

Received: April 27, 2023
Revised: July 19, 2023
Published online:

[1] M. Wei, Y. Gao, X. Li, M. J. Serpe, *Polym. Chem.* **2016**, *8*, 127.
[2] A. S. Hoffman, *Adv. Drug Delivery Rev.* **2013**, *65*, 10.
[3] S. S. Das, P. Bharadwaj, M. Bilal, M. Barani, A. Rahdar, P. Taboada, S. Bungau, G. Z. Kyzas, *Polymers* **2020**, *12*, 1397.
[4] M. C. Koetting, J. T. Peters, S. D. Steichen, N. A. Peppas, *Mater Sci Eng R Rep* **2015**, *93*, 1.
[5] N. Sood, A. Bhardwaj, S. Mehta, A. Mehta, *Drug Delivery* **2016**, *23*, 748.
[6] M. Toma, U. Jonas, A. Mateescu, W. Knoll, J. Dostalek, *J Phys Chem C Nanomater Interfaces* **2013**, *117*, 11705.
[7] Y. Wang, P. Feng, R. Liu, B. Song, *Sens Actuators B Chem* **2021**, *330*, 129236.
[8] Y. Xia, Y. He, F. Zhang, Y. Liu, J. Leng, *Adv. Mater.* **2021**, *33*, 2000713.
[9] X. Deng, J. L. Livingston, N. J. Spear, G. K. Jennings, *Langmuir* **2020**, *36*, 715.
[10] S. Dai, P. Ravi, K. Chiu Tam, K. C. Tam, *Soft Matter* **2008**, *4*, 435.
[11] Y. J. Kim, Y. T. Matsunaga, *J. Mater. Chem. B* **2017**, *5*, 4307.
[12] D. Szabo, G. Szeghy, M. Zrinyi, *Macromolecules* **1998**, *31*, 6541.
[13] G. Filipcsei, J. Feher, M. Zrinyi, *J. Mol. Struct.* **2000**, *554*, 109.
[14] R. Das, M. Kuehnert, A. S. Kazemi, Y. Abdi, A. Schulze, *Polymers* **2019**, *11*, 344.
[15] L. Y. Chu, Y. Li, J. H. Zhu, H. D. Wang, Y. J. Liang, *J Control Release* **2004**, *97*, 43.
[16] T. Uemukai, M. Torisaki, T. Hamanaka, M. Ishifune, *J. Appl. Polym. Sci.* **2013**, *130*, 3458.
[17] X. Xu, Y. Liu, W. Fu, M. Yao, Z. Ding, J. Xuan, D. Li, S. Wang, Y. Xia, M. Cao, *Polymers* **2020**, *12*, 580.
[18] D. Han, X. Tong, O. Boissière, Y. Zhao, *ACS Macro Lett.* **2012**, *1*, 57.
[19] K. Zhang, M. Zhang, X. Feng, M. A. Hempenius, G. J. Vancso, K. Zhang, M. A. Hempenius, G. J. Vancso, M. Zhang, X. Feng, *Adv. Funct. Mater.* **2017**, *27*, 1702784.
[20] M. Benoit, D. Bouyer, P. Sistat, A. Ayral, D. Cot, B. Rebiere, D. Fournier, J. Lyskawa, P. Woisel, C. Antonelli, D. Quemener, *Chem. Mater.* **2021**, *33*, 998.
[21] J. Pirkin-Benameur, D. Bouyer, D. Quemener, *J Memb Sci* **2022**, *658*, 120742.
[22] B. P. Belousov, *Sbornik Referatov po Radiatsionni Meditsine* **1958**, 145.
[23] A. M. Zhabotinsky, *Biofizika* **1964**, *9*, 306.
[24] A. M. Zhabotinsky, *Dokl Akad Nauk SSSR* **1964**, *157*, 392.
[25] I. R. Epstein, J. A. Pojman, *An Introduction to Nonlinear Chemical Dynamics: Oscillations, Waves, Patterns and Chaos*, Oxford University Press, New York, **1998**.
[26] J. A. Pojman, Q. Tran-Cong-Miyata, *Nonlinear Dynamics with Polymers: Fundamentals, Methods and Applications*, WILEY-VCH Verlag GmbH & Co. KGaA, Weinheim, **2010**.
[27] J. A. Pojman, D. C. Leard, W. West, *J. Am. Chem. Soc.* **1992**, *114*, 8298.
[28] R. P. Washington, G. P. Misra, W. W. West, J. A. Pojman, *J. Am. Chem. Soc.* **1999**, *121*, 7373.
[29] F. Gauffre, V. Labrot, J. Boissonade, P. De Kepper, *Spontaneous Deformations in Polymer Gels Driven by Chemomechanical Instabilities: in Nonlinear Dynamics in Polymeric Systems*, Acs Symposium Series No. 869, (Eds.: J. A. Pojman, Q. Tran-Cong-Miyata), American Chemical Society, Washington, DC, **2003**, pp 80-93.
[30] V. Labrot, P. De Kepper, J. Boissonade, I. Szalai, F. Gauffre, *J. Phys. Chem. B* **2005**, *109*, 21476.
[31] J. Horváth, I. Szalai, J. Boissonade, P. De Kepper, *Soft Matter* **2011**, *7*, 8462.
[32] E. Jee, T. Bánsági, A. F. Taylor, J. A. Pojman, *Angew. Chem., Int. Ed.* **2016**, *55*,2127.
[33] T. Ueki, R. Yoshida, *Phys. Chem. Chem. Phys.* **2014**, *16*, 10388.
[34] R. Yoshida, *Biophysics* **2012**, *8*, 163.
[35] R. Yoshida, T. Sakai, Y. Hara, S. Maeda, S. Hashimoto, D. Suzuki, Y. Murase, *J. Controlled Release* **2009**, *140*, 186.
[36] R. Yoshida, *Adv. Mater. Lett.* **2018**, *9*, 836.
[37] R. Yoshida, T. Takahashi, T. Yamaguchi, T. Yamaguchi, H. Ichijo, *Adv. Mater.* **1997**, *9*, 175.
[38] S. Maeda, Y. Hara, T. Sakai, R. Yoshida, S. Hashimoto, *Adv. Mater.* **2007**, *19*, 3480.
[39] Y. Murase, S. Maeda, S. Hashimoto, R. Yoshida, *Langmuir* **2009**, *25*, 483.
[40] O. Tabata, H. Hirasawa, S. Aoki, R. Yoshida, E. Kokufuta, *Sensors Actuators A Phys* **2002**, *95*, 234.
[41] Y. Shiraki, R. Yoshida, *Angew. Chem., Int. Ed.* **2012**, *51*, 6112.
[42] Y. Hara, H. Mayama, K. Fujimoto, *J Phys Chem B* **2014**, *118*, 6931.
[43] Y. Hara, K. Fujimoto, H. Mayama, *J Phys Chem B* **2014**, *118*, 608.
[44] A. H. Taheri, L. N. Sim, W. B. Krantz, A. G. Fane, *Sep. Purif. Technol.* **2019**, *212*, 262.

© 2023 The Authors. Advanced Materials Interfaces published by Wiley-VCH GmbH

21967350, 0, Downloaded from https://onlinelibrary.wiley.com/doi/10.1002/admi.202300346 by Cochrane France, Wiley Online Library on [05/09/2023]. See the Terms and Conditions (https://onlinelibrary.wiley.com/terms-and-conditions) on Wiley Online Library for rules of use; OA articles are governed by the applicable Creative Commons License

[45] C. Li, D. Zhang, J. Liu, H. Xiong, T. Sun, X. Wu, Z. Shi, Q. Lin, *Membranes* **2022**, *12*, 362.
[46] T. Masuda, A. Terasaki, A. M. Akimoto, K. Nagase, T. Okano, R. Yoshida, *RSC Adv.* **2015**, *5*, 5781.
[47] T. Masuda, A. M. Akimoto, M. Furusawa, R. Tamate, K. Nagase, T. Okano, R. Yoshida, *Langmuir* **2018**, *34*, 1673.
[48] Y. Hara, *Key Eng Mater* **2011**, *480*, 369.
[49] Y. Hara, R. A. Jahan, *Key Eng Mater* **2011**, *467*, 1472.
[50] K. Miyakawa, K. Miyakawa, F. Sakamoto, R. Yoshida, E. Kokufuta, T. Yamaguchi, T. Yamaguchi, *Phys Rev E* **2000**, *62*, 793.
[51] Y. Hara, *Chemosens* **2013**, *1*, 3.
[52] T. Geher-Herczegh, Z. Wang, T. Masuda, R. Yoshida, N. Vasudevan, Y. Hayashi, *Macromolecules* **2021**, *54*, 6430.
[53] B. A. Humphreys, E. J. Wanless, G. B. Webber, *J. Colloid Interface Sci.* **2018**, *516*, 153.
[54] C. Zobrist, J. Sobocinski, J. Lyskawa, D. Fournier, V. Miri, M. Traisnel, M. Jimenez, P. Woisel, *Macromolecules* **2011**, *44*, 5883.
[55] H. Rothfuss, N. D. Knöfel, P. Tzvetkova, N. C. Michenfelder, S. Baraban, A.-N. Unterreiner, P. W. Roesky, C. Barner-Kowollik, *Chemistry* **2018**, *24*, 17475.
[56] H. Lee, S. M. Dellatore, W. M. Miller, P. B. Messersmith, *Science* **2007**, *318*, 426.

© 2023 The Authors. Advanced Materials Interfaces published by Wiley-VCH GmbH

21967350, 0, Downloaded from https://onlinelibrary.wiley.com/doi/10.1002/admi.202300346 by Cochrane France, Wiley Online Library on [05/09/2023]. See the Terms and Conditions (https://onlinelibrary.wiley.com/terms-and-conditions) on Wiley Online Library for rules of use; OA articles are governed by the applicable Creative Commons License